



ARTICLE

## MHD (SWCNTS + MWCNTS)/H<sub>2</sub>O-Based Williamson Hybrid Nanofluids Flow Past Exponential Shrinking Sheet in Porous Medium

Hamzeh Taha Alkawasbeh<sup>1,\*</sup> and Muhammad Khairul Anuar Mohamed<sup>2</sup>

<sup>1</sup>Department of Mathematics, Faculty of Science, Ajloun National University, P.O. Box 43, Ajloun, 26810, Jordan

<sup>2</sup>Centre for Mathematical Sciences, Universiti Malaysia Pahang, Persiaran Lebuhraya Tun Khalil Yaakob, Kuantan, Pahang, 26300, Malaysia

\*Corresponding Author: Hamzeh Taha Alkawasbeh. Email: hamzahtahak@yahoo.com

Received: 26 April 2023 Accepted: 09 June 2023

### ABSTRACT

The present study numerically investigates the flow and heat transfer of porous Williamson hybrid nanofluid on an exponentially shrinking sheet with magnetohydrodynamic (MHD) effects. The nonlinear partial differential equations which governed the model are first reduced to a set of an ordinary differential equations by using the similarity transformation. Next, the BVP4C solver is applied to solving the equations by considering the pertinent fluid parameters such as the permeability parameter, the magnetic parameter, the Williamson parameter, the nanoparticle volume fractions and the wall mass transfer parameter. The single (SWCNTs) and multi-walled carbon nanotubes (MWCNTs) nanoparticles are taken as the hybrid nanoparticles. It is found that the increase in magnetic parameter in SWCNT + MCWNT hybrid nanofluid results to the increase of 72.2% on skin friction compared to SWCNT nanofluid while maintaining reducing a small number of Nusselt number. This shows the potential of the Williamson hybrid nanofluid as a friction application purposes especially in transportation like braking system, flushing fluid and mechanical engineering.

### KEYWORDS

Hybrid nanofluid; MHD; porous medium; BVP4C method

### Nomenclature

$B_0$	Magnetic field strength, $Wb$
$C_f$	Local skin friction coefficient
$c_p$	Specific heat capacity, $Jkg^{-1}K^{-1}$
$K$	Permeability parameter, $tma^{-1}$
$K$	Variable permeability of porous medium
$\ell$	Length of sheet, $M$
$M$	Magnetic parameter
$Nu$	Nusselt number
$Pr$	Prandtl number
$\bar{q}$	Heat flux, $Wm^{-2}$



$Re$	Local reynolds number
$S$	Wall mass transfer parameter
$T$	Temperature, $K$
$T_o$	Reference temperature, $K$
$u_w$	Variable shrinking velocity, $Ms^{-1}$
$V_w$	Variable velocity of suction/injection, $Ms^{-1}$
$v_1$	Velocity component along $x$ -axis, $Ms^{-1}$
$v_2$	Velocity component along $Y$ -axis, $Ms^{-1}$
$We$	Williamson parameter
$\mu$	Dynamic viscosity, $Kgm^{-1}s^{-1}$
$\nu$	Kinematic viscosity, $M^2s^{-1}$
$P$	Density, $Kgm^{-3}$
$\Sigma$	Electrical conductivity, $A^2s^3kg^{-1}m^{-3}$
$\Psi$	Stream function, $Kgm^{-1}s^{-1}$
$\bar{\tau}_x$	Wall shear stress, $Kgm^{-1}s^{-2}$
$\chi$	Nanoparticle volume fraction

### Subscripts

$f$	Base fluid
$SW$	SWCNTs
$MW$	MWCNTs
$hnf$	Hybrid Nanofluid
$w$	Wall/Surface
$\infty$	Ambient Environment

## 1 Introduction

Nanofluid played a vital role in industrial and automotive applications. It is widely used as the radiator coolant, brake fluid and as a smart fluid in battery devices. Nanofluid is also applied as a coolant medium at a nuclear reactors, geothermal power, tire plant as well as in very small electronic applications such as microchip coolers [1].

Historically, the term nanofluid has first been coined by Choi et al. [2] to express the term nanofluid (nanoparticles fluid suspension). The nano size (<100 nm) solid particles in the fluid later known as the nanoparticles are usually made from metal or oxide. Metal nanoparticles such as zinc Zn, copper Cu and silver Ag are popular because of their high in thermal conductivities [3–5]. On the other side, these metal nanoparticles are high in density and thus promoted high friction between fluid and surface which cause corrosion. Furthermore, it is expensive. Meanwhile, the oxide nanoparticles are cheap and economical to be produced in mass production, but the oxide nanoparticles have low thermal conductivities. Increasing the percentage of nanoparticles in the fluid may increase the thermal behavior performance, but too many nanoparticles in the fluid will promote clogging.

Hybrid nanofluids can be considered as a new generation of Nanofluids. It is a very new idea. This is the composition of two variant types of dispersed nanoparticles in base fluids. This phenomenon have tale features that might make them helpful in many heat transfer organizations, like microelectronics, components of energy, pharmaceutical equipment, half breed powdered engines, engine cooling, car warming Administration, home cooler, chiller, thermal exchanger, atomic reactor coolant, grinding machinery, space innovation [6]. Sundar et al. [7] have proposed a thorough process

for generating hybrid nanofluids, including their advantages and disadvantages. Waini et al. [8] have investigated the stretching and contracting of a sheet-induced hybrid nanofluid created by adding copper nanoparticles to an  $\text{Al}_2\text{O}_3/\text{water}$  nanofluid. To explore the impact of thermal radiation, chemical reaction, suction, and slip condition on the heat and mass transfer of an unsteady MHD flow across a stretched surface, researchers Sreedevi et al. [9] have combined both carbon nanotubes and silver nanoparticles in the base fluid (water). The influence of radiation and suction on the dynamics of an MHD hybrid nanofluid moving through a stretching sheet has been studied by Yashkun et al. [10].

With the rising era of graphene, the carbon nanotube (CNT) seems to be the alternative for the high-density issue of metal nanoparticles while providing better thermal conductivity than oxide nanoparticles. Anuar et al. [11] studied the stability analysis of flow and heat transfer of carbon nanotubes over a moving plate. The heat transfer capabilities between the single (SWCNTs) and multi-walled carbon nanotubes (MWCNTs) nanoparticles in water as a based fluid are numerically examined. Next, Hayat et al. [12] investigated the carbon nanotube effects represented by SWCNTs and MWCNTs nanoparticles in the melting heat transfer over an impermeable stretchable surface in a nanofluid. Zaki et al. [13] concluded that the presence of SWCNTs nanoparticles in the Cu/water nanofluid so-called SWCNTs-Cu/water hybrid nanofluid dramatically raised the surface temperature and the heat transfer coefficient. Recently, Idrees et al. [14] studied the 3D rotational flow and heat transfer dynamics of a hybrid (SWCNT-MWCNT) nanofluid.

Considering the stretching/shrinking sheet in industrial processes, the heat transfer rate on the stretching/shrinking components plays an important factor in the quality of the product produces. Since half a century ago, the investigation of convection flow past a stretching/shrinking sheet has attracted the researcher's attention [15]. The investigation evolved by including various physical external forces on a fluid flow such as the magnetic effects, the thermal radiation effects, the chemical reaction, the viscous dissipation, the heat generation/absorption and the permeability effects [16–20]. Recently, the bio-convection and activation energy across of Prandtl nanofluid flow on a stretching cylinder has been investigated by Shah et al. [21].

The study flows on a stretching sheet then are extended by considering the industrial fluid such as the Maxwell fluid, the Williamson hybrid ferrofluid, the micropolar nanofluid, the second-grade nanofluid, the Casson nanofluid and the viscoelastic nanofluid as recently studied by [22–28].

Motivated by the above literature, the present study investigates the carbon nanotube Williamson hybrid nanofluid flow on an exponentially stretching sheet with MHD effects. The SWCNTs and MWCNTs nanoparticles are taken as the hybrid particles. Such investigation has never been done before, so the reported result in this study is new. This research will be answering whether the blended carbon nanotube performs better than the single carbon nanotube nanofluid and the effects of the magnetic, shrinking surface, and the porosity in the fluid on the fluid flow and heat transfer performance.

## 2 Mathematical Formulations

Consider a steady 2-dimensional Williamson hybrid nanofluid boundary layer flow with single (SWCNTs) and multi-walled carbon nanotubes (MWCNTs) nanoparticles with water  $\text{H}_2\text{O}$  as a based-fluid on an exponentially shrinking sheet. The porous surface is considered, with variable wall mass suction/injection applied through it. Fig. 1 shows a physical representation of this situation. Physical model of the fluid flow can be modelled to a basic equation for motion and energy distribution are as follows [28]:

$$\frac{\partial v_1}{\partial x} + \frac{\partial v_2}{\partial y} = 0, \quad (1)$$

$$v_1 \frac{\partial v_1}{\partial x} + v_2 \frac{\partial v_1}{\partial y} = \frac{\mu_{hmf}}{\rho_{hmf}} \left( \frac{\partial^2 u_1}{\partial y^2} - \frac{v_1}{k^*} \right) - \frac{\sigma_{hmf}}{\rho_{hmf}} B_0^2 v_1 + \sqrt{2} \Gamma \frac{\partial v_1}{\partial y} \frac{\partial^2 v_1}{\partial y^2}, \quad (2)$$

$$v_1 \frac{\partial T}{\partial x} + v_2 \frac{\partial T}{\partial y} = \frac{k_{hmf}}{(\rho C_p)_{hmf}} \frac{\partial^2 T}{\partial y^2}, \quad (3)$$

subjected to

$$v_1 = -u_w(x) = ae^{x/2\ell}, \quad v_2 = -V_w(x) = V_0 e^{x/2\ell} \quad T = T_w = T_\infty + T_o e^{x/2\ell} \quad \text{at } y = 0, \quad (4)$$

$$v_1 \rightarrow 0, \quad T \rightarrow T_\infty \quad \text{as } y \rightarrow \infty,$$

where  $v_1$  and  $v_2$  denotes respectively velocity components along  $x$ - and  $y$ -directions,  $k = k_o/e^{x/2\ell}$  gives variable permeability of porous medium with  $k_o$  being a non-negative constant,  $T$  represents temperature of hybrid nanofluid,  $u_w = ae^{x/2\ell}$  is variable shrinking velocity with  $a$  being positive constant having dimension  $\ell T^{-1}$ . Next,  $V_w = V_0 e^{x/2\ell}$  is variable velocity of suction/injection,  $T_o$  and  $\ell$  denote reference temperature and length. Furthermore,  $(\rho_{hmf})$ ,  $(\mu_{hmf})$ ,  $(\sigma_{hmf})$ ,  $(k_{hmf})$ , and  $(\rho c_p)_{hmf}$  are the density, dynamic viscosity, electrical conductivity, thermal conductivity and heat capacity of hybrid nanofluid, respectively, which are defined as [29].

$$\rho_{hmf} = (1 - \chi_{SW}) [(1 - \chi_{MW}) \rho_f + \chi_{SW} \rho_{SW}] + \chi_{MW} \rho_{MW},$$

$$\mu_{hmf} = \frac{\mu_f}{(1 - \chi_{SW})^{2.5} (1 - \chi_{MW})^{2.5}},$$

$$(\rho c_p)_{hmf} = (1 - \chi_{MW}) [(1 - \chi_{SW}) (\rho c_p)_f + \chi_{SW} (\rho c_p)_{SW}] + \chi_{MW} (\rho c_p)_{MW},$$

$$\frac{k_{hmf}}{k_{bf}} = \frac{(k_{MW} + 2k_{bf}) - 2\chi_{MW} (k_{bf} - k_{MW})}{(k_{MW} + 2k_{bf}) + \chi_{MW} (k_{bf} - k_{MW})},$$

where

$$\frac{k_{bf}}{k_f} = \frac{(k_{SW} + 2k_f) - 2\chi_{SW} (k_f - k_{SW})}{(k_{SW} + 2k_f) + \chi_{SW} (k_f - k_{SW})},$$

$$\alpha_{hmf} = \frac{k_{hmf}}{(\rho c_p)_{hmf}},$$

$$\frac{\sigma_{hmf}}{\sigma_f} = 1 + \frac{3 \left[ \frac{\chi_{SW} \sigma_{SW} + \chi_{MW} \sigma_{MW}}{\sigma_f} - (\chi_{SW} + \chi_{MW}) \right]}{\left[ \frac{\chi_{SW} \sigma_{SW} + \chi_{MW} \sigma_{MW}}{\sigma_f} + 2 \right] - \left[ \frac{\chi_{SW} \sigma_{SW} + \chi_{MW} \sigma_{MW}}{\sigma_f} - (\chi_{SW} + \chi_{MW}) \right]}.$$

Note that the properties related to base fluid, the SWCNTs and MWCNTs nanoparticles are denoted with subscript  $_f,_{SW}$  and  $_{MW}$ . Next, the continuity Eq. (1) is satisfied with the introduction of

the stream function  $\Psi$  so that  $v_1 = \frac{\partial \Psi}{\partial y}$  and  $v_2 = -\frac{\partial \Psi}{\partial x}$ . To simply, the dependent variable in Eqs. (2) and (3) can be reduced. It is introduced the following self-similar transformations:

$$\begin{aligned} v_1 &= ae^{x/\ell} F'(\eta), \quad v_2 = -\sqrt{\frac{av_f}{2\ell}} (F(\eta) + \eta F'(\eta)), \\ \theta(\eta) &= \frac{T - T_\infty}{T_w - T_\infty}, \quad \eta = ye^{x/2\ell} \sqrt{\frac{a}{2\ell v_f}}. \end{aligned} \quad (5)$$

Using Eq. (5), the Eqs. (2) and (3) can be expressed in the form of self-similar nonlinear equations as follows:

$$\frac{P_1}{P_2} (F''' - KF') + FF'' - 2(F')^2 - \frac{P_3}{P_2} MF' + WeF''F''' = 0, \quad (6)$$

$$P_4 \theta'' + \text{Pr} (F\theta' - F'\theta) = 0, \quad (7)$$

where  $K = \frac{2\ell v_f}{ak^*}$  is the permeability parameter,  $\text{Pr} = \frac{v_f(\rho C_p)_f}{k_f}$  is the Prandtl number.

$We = x\sqrt{2\ell}\Gamma\sqrt{\frac{a^3}{v_f}}$  is the Weissenberg number and  $M = \left(\frac{\sigma_f B_0^2}{a\rho_f}\right)$  is the magnetic parameter. Also

$$P_1 = \frac{1}{(1 - \chi_{SW})^{2.5} (1 - \chi_{MW})^{2.5}},$$

$$P_2 = (1 - \chi_{SW}) [(1 - \chi_{MW}) \rho_f + \chi_{SW} \rho_{SW}] + \chi_{MW} \rho_{MW},$$

$$P_3 = 1 + \frac{3 \left[ \frac{\chi_{SW} \sigma_{SW} + \chi_{MW} \sigma_{MW}}{\sigma_f} - (\chi_{SW} + \chi_{MW}) \right]}{\left[ \frac{\chi_{SW} \sigma_{SW} + \chi_{MW} \sigma_{MW}}{\sigma_f} + 2 \right] - \left[ \frac{\chi_{SW} \sigma_{SW} + \chi_{MW} \sigma_{MW}}{\sigma_f} - (\chi_{SW} + \chi_{MW}) \right]},$$

$$P_4 = \frac{k_{mf}/k_{bf}}{(1 - \chi_{MW}) [(1 - \chi_{SW})(\rho c_p)_f + \chi_{SW}(\rho c_p)_{SW}/(\rho c_p)_f] + \chi_{MW}(\rho c_p)_{MW}/(\rho c_p)_f}.$$

The boundary conditions in Eq. (4) is reduced to the following forms:

$$\begin{aligned} F = S, F' = -1, \quad \theta = 1, \quad \text{at} \quad \eta = 0, \\ F' \rightarrow 0, \quad \theta \rightarrow 0, \quad \text{as} \quad \eta \rightarrow \infty. \end{aligned} \quad (8)$$

Here,  $S = V_0\sqrt{2\ell/av_f}$  is the wall mass transfer parameter, The physical quantities interested in this study are the local skin friction coefficient  $Cf$  and the Nusselt number  $Nu$  which can be expressed as [28]

$$Cf = \frac{\bar{\tau}_x}{\rho_{mf} U_w^2}, \quad Nu = \frac{x\bar{q}_w}{k_f(T_w - T_\infty)}, \quad (9)$$

where

$$\bar{\tau}_x = \mu_{mf} \left( \frac{\partial v_1}{\partial y} \right)_{y=0}, \quad \bar{q}_w = -k_{mf} \left( \frac{\partial T}{\partial y} \right)_{y=0}. \quad (10)$$

Using the definitions described above then the  $Cf$  and  $Nu$  are reduced as

$$\sqrt{\text{Re}} Cf = \frac{K_1}{K_2} [F''(0) + We(F''(0))^2], \quad \frac{Nu}{\sqrt{\text{Re}}} = -\frac{k_{mf}}{k_f} \theta'(0). \quad (11)$$

with  $\sqrt{Re} = x \sqrt{\frac{a}{\nu_f}}$  where  $Re$  is the local Reynolds number.

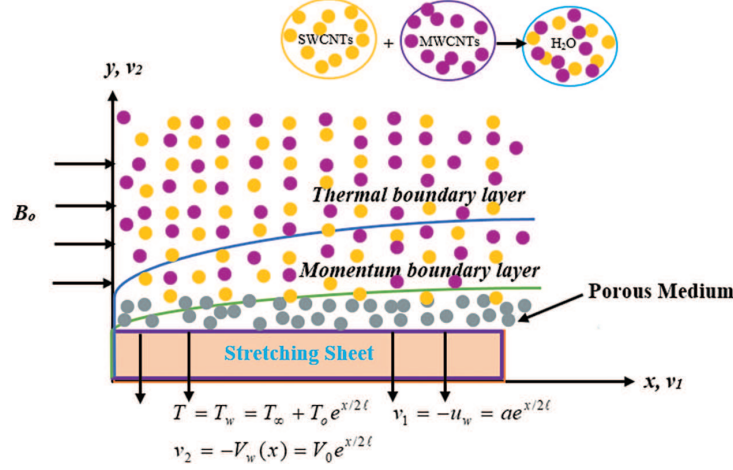


Figure 1: Physical geometry of the fluid flow

### 3 Numerical Simulation

The transformed ordinary differential Eqs. (6) and (7) with the boundary conditions (8) were solved numerically considering the water-based Williamson nanofluid SWCNTs/H<sub>2</sub>O and the water-based Williamson hybrid nanofluid (SWCNTs + MWCNTs)/H<sub>2</sub>O. Results from the study are presented in a graphic and tabular format, with a focus on the model's mathematical components and their effects on velocity, temperature, and physical interest quantities. This study used the numerical technique from `bvp4c` function in MATLAB. `bvp4c` is the finite difference code implements the well-known three-stage Lobatto IIIA formula. Named after Reuel Lobatto, this method is a collocation formula as Runge-Kutta method and provides a fourth-order accurate uniformly results. Related works that implements the `bvp4c` method included [30,31] and recently by [32,33].

To use this approach, the transformed ordinary differential equations are converted into the system of 1st order differential equations, which is followed as

$$\begin{cases} y_1 = F, y_2 = F', y_3 = F'', yy_a = F''', \\ y_4 = \theta, y_5 = \theta', yy_b = \theta'' \end{cases} \quad (12)$$

with

$$yy_a = \left[ 1 / \left( \left( \frac{P_1}{P_2} \right) - We y_3 \right) \right] \left[ \left( \frac{P_1}{P_2} \right) K y_2 + 2 y_2^2 + \left( \frac{P_3}{P_2} \right) M y_2 \right] \quad (13)$$

$$yy_b = - \left( \frac{Pr}{P_4} \right) [y_1 y_5 - y_2 y_4]. \quad (14)$$

Corresponding boundary condition are converted as

$$\begin{cases} y_1(0) - S \\ y_2(0) + 1 \\ y_2(\infty) \end{cases} \quad (15)$$

$$\begin{cases} y_4(0) - 1 \\ y_4(\infty) \end{cases}$$

The resulting transformation above with the suitable IVP are coded into MATLAB software to compute numerically, see [Fig. 2](#).

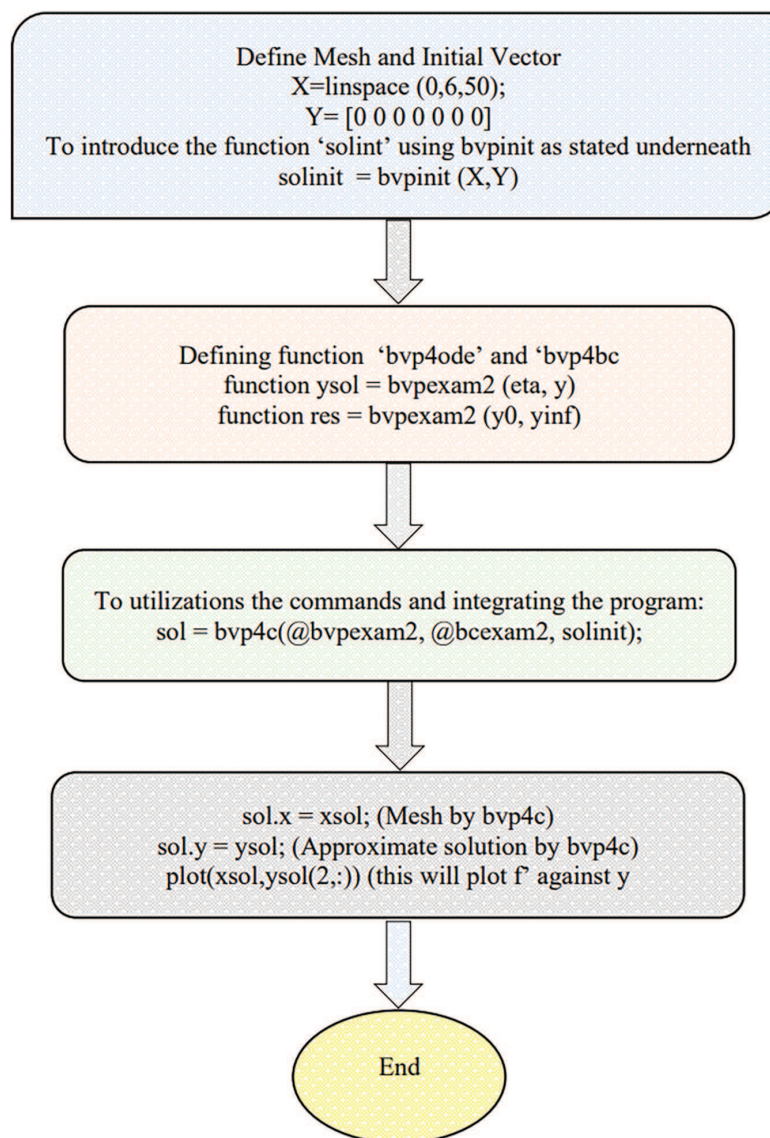


**Figure 2:** Flow chart of bvp4c method

#### 4 Results and Discussion

The transformed ordinary differential Eqs. (6) and (7) with boundary conditions (8) were solved numerically using the BVP4C function in MATLAB software. The numerical computation considers the changes of pertinent parameters such as the permeability parameter  $K$ , the magnetic parameter  $M$ , the Williamson parameter  $We$ , the nanoparticle volume fractions of SWCNTs  $\chi_{SW}$  and MWCNTs nanoparticles  $\chi_{MW}$ , respectively and the wall mass transfer parameter  $S$  in the fluid flow. Further, the Prandtl number  $Pr$  is taken as 7 considering the  $Pr$  values for water. Table 1 shows the thermo-physical properties of water as a based fluid with carbon nanotube nanoparticles.

**Table 1:** Thermo-physical properties of water and carbon nanotube nanoparticles [13,14]

Thermo-physical properties	$\rho$ (kg m <sup>-3</sup> )	$C_p$ (J k g <sup>-1</sup> K <sup>-1</sup> )	$k$ (W m <sup>-1</sup> K <sup>-1</sup> )	$\sigma$ (S m <sup>-1</sup> )
H <sub>2</sub> O	997.1	4179	0.613	$5.5 \times 10^{-6}$
SWCNTs	2600	425	6600	$10^{-6}$
MWCNTs	1600	796	3000	$1.9 \times 10^{-4}$

The effects of fluid parameters on the reduced skin friction coefficient  $\sqrt{Re}Cf$  is tabulated in Table 2. From Table 2, it is found that the increase in magnetic parameter  $M$ , the permeability parameter  $K$ , the nanoparticle volume fractions of MWCNTs  $\chi_{MW}$  and the wall mass transfer parameter  $S$  results in enhanced friction between the fluid and the plate surface. This is physically realistic due to the effects of  $M$  and  $K$  attracting the fluid particle or giving the suction effects towards the plate surface which contributing extra force from fluid to a surface thus increased friction. Meanwhile, the increase in Williamson parameter  $We$  have reduced the skin friction coefficient. Crossing Table 2, it is concluded that, the water-based Williamson hybrid nanofluid (SWCNTs + MWCNTs)/H<sub>2</sub>O produced high in  $\sqrt{Re}Cf$  values compared to the water-based Williamson nanofluid SWCNTs/H<sub>2</sub>O.

**Table 2:** Influence of  $M$ ,  $K$ ,  $We$ ,  $S$  and  $\chi_{MW}$  on  $\sqrt{Re}Cf$

$M$	$K$	$S$	$\chi_{MW}$	$We$	(SWCNTs + MWCNTs)/H <sub>2</sub> O	(SWCNTs)/H <sub>2</sub> O
1	1	2		1	2.7557	1.8173
2					3.3411	2.0245
3					3.7808	2.1953
1	1	2		1	2.7557	1.8173
		2			2.9608	2.1088
		3			3.1423	2.3355
1	1	2		1	2.7557	1.8173
		3			3.0631	2.2108
		4			3.3751	2.5909
1	1	2		1	2.7557	1.8173
				2	2.3332	1.5258
				3	2.0892	1.3565
			0.05		1.5557	—

(Continued)

**Table 2 (continued)**

$M$	$K$	$S$	$\chi_{MW}$	$We$	(SWCNTs + MWCNTs)/H <sub>2</sub> O	(SWCNTs)/H <sub>2</sub> O
			0.1	3	2.0892	–
			0.2		2.8384	–

Table 3 tabulated the effects of fluid parameters on the reduced Nusselt number  $Nu/\sqrt{Re_x}$ . It is suggested that a small increment on  $Nu/\sqrt{Re_x}$  was found as  $M$  and  $K$  increased. On the other hand, the increase in  $S$  has boosting the values of  $Nu/\sqrt{Re_x}$  drastically. Physically the suction effect produced by the wall mass transfer parameter  $S$  reduced the fluid particle, providing the convection process between the fluid and plate surface occurs effectively thus boosted the reduced Nusselt number  $Nu/\sqrt{Re_x}$ . Meanwhile, the increase in Williamson parameter  $We$  and  $\chi_{MW}$  has slightly reduced the values of  $Nu/\sqrt{Re_x}$ . Comparing the performance between the nanofluid, the water-based Williamson hybrid nanofluid (SWCNTs + MWCNTs)/H<sub>2</sub>O has lower in  $Nu/\sqrt{Re_x}$  values compared to the water-based Williamson nanofluid SWCNTs/H<sub>2</sub>O. Physically, carbon nanotube nanoparticles have high thermal conductivity properties. The increase in carbon nanotube nanoparticles in the fluid has enhanced the fluid thermal conductivity, thus raising the fluid conductive properties, therefore reducing the convective heat transfer capabilities of the fluid.

**Table 3:** Influence of  $M$ ,  $K$ ,  $We$ ,  $S$  and  $\chi_{MW}$  on  $Nu/\sqrt{Re_x}$ 

$M$	$K$	$S$	$\chi_{MW}$	$We$	(SWCNTs + MWCNTs)/H <sub>2</sub> O	(SWCNTs)/H <sub>2</sub> O
1	1	2		1	11.3665	11.5472
2					11.4083	11.5586
3					11.5472	11.5677
1	1	2		1	11.3665	11.5472
		2			11.3816	11.5631
		3			11.3946	11.5750
1	1	2		1	11.3665	11.5472
		3			17.9208	18.0513
		4			24.2903	24.3920
1	1	2		1	11.3665	11.5472
				2	11.3352	11.5310
				3	11.3155	11.5210
			0.05		11.4248	–
			0.1	3	11.3155	–
			0.2		11.0460	–

In discussing the fluid flow behavior across the boundary layer, Figs. 3–7 are illustrated. From Figs. 3 and 5, it is found that the increase of  $M$ ,  $K$  and  $S$  has slightly increased the fluid flow velocity while reducing the velocity boundary layer thickness. The reduction in the thickness of the boundary layer physically leads to the increase in velocity gradient which derives to the increase in skin friction

coefficient as found in Table 2. The same pattern occurs in Fig. 7 where the increase in  $\chi_{MW}$  results in an increase in velocity distribution while reducing the boundary layer thickness. The increase in  $\chi_{MW}$  enhanced the fluid momentum thus speeds up the fluid flow velocity. This outcome is agreed by the fluid comparison achieved in Figs. 3–6 where the water-based Williamson hybrid nanofluid (SWCNTs + MWCNTs)/H<sub>2</sub>O has higher fluid flow velocity as well as the skin friction coefficient compared to the water-based Williamson nanofluid SWCNTs/H<sub>2</sub>O. Meanwhile, the Williamson parameter  $We$  gives negative effects on the fluid flow. As seen in Fig. 6, it is found that the velocity distribution decreases as the  $We$  increases.

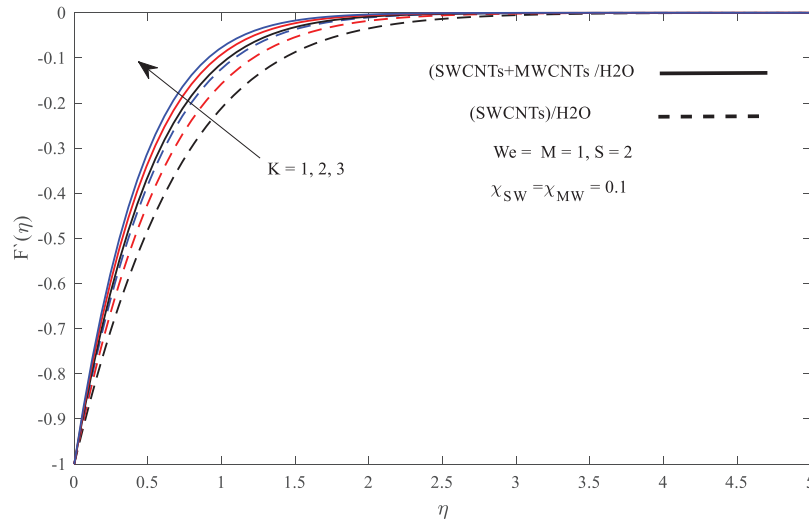


**Figure 3:** Influence of  $K$  on velocity profiles  $F'(\eta)$

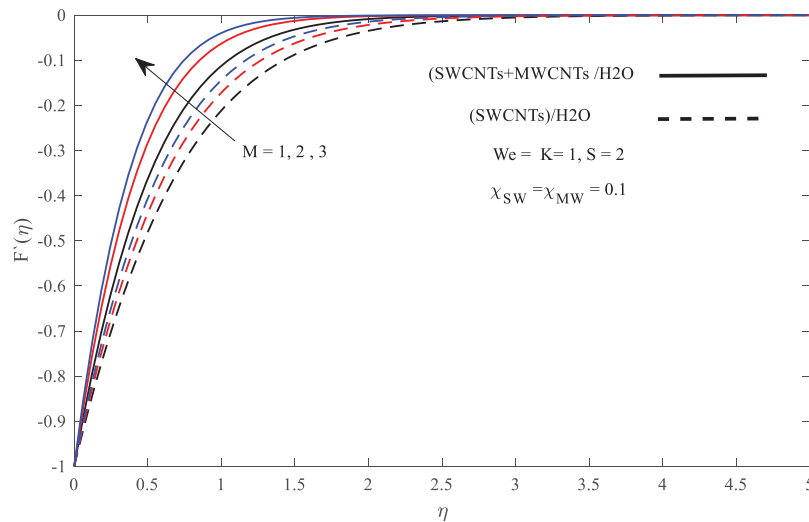


**Figure 4:** Influence of  $M$  on velocity profiles  $F'(\eta)$

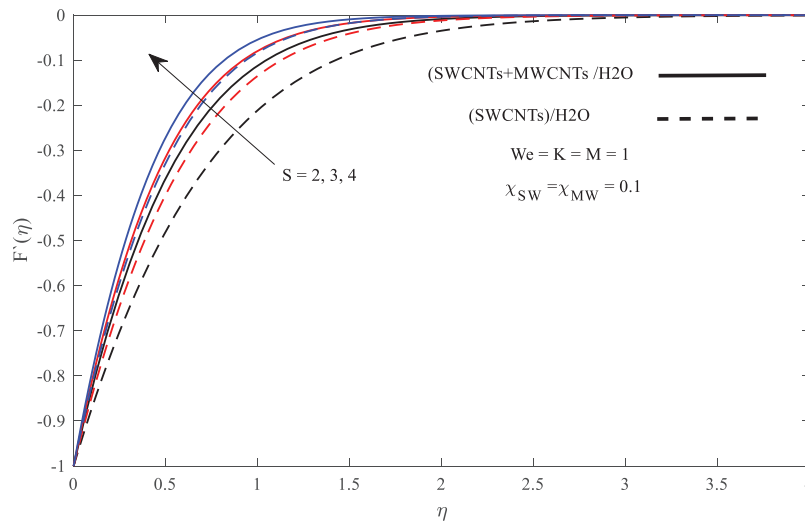


**Figure 5:** Influence of  $S$  on velocity profiles  $F'(\eta)$

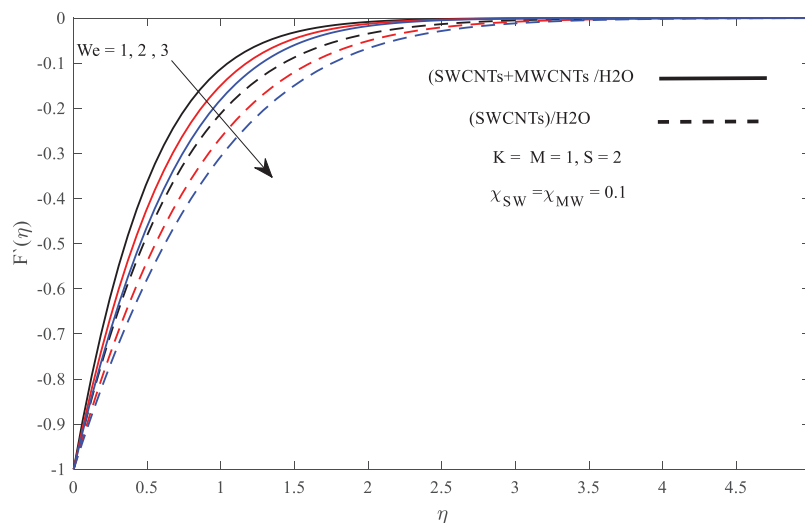


**Figure 6:** Influence of  $We$  on velocity profiles  $F'(\eta)$

Lastly, Figs. 8 and 9 depicted the temperature profiles  $\theta(\eta)$  for different values of  $S$  and  $\chi_{MW}$ , respectively. From Fig. 8, it is observed that the increase in  $S$  results in a reduction in the thermal boundary layer thickness. This implies shortening the depth for the fluid with wall temperature to achieve the stream temperature outside the boundary layer. Shortening the thickness refers to the increase in the temperature gradient, thus physically reflecting the increase in Nusselt number as supported by Table 3. Meanwhile, the increase in  $\chi_{MW}$  in Fig. 8 has widened the thermal boundary layer thickness as well as the temperature distributions. This is realistic because the increase in  $\chi_{MW}$  leads to an increase in nanofluid thermal conductivities, thus enhancing the fluid thermal capabilities. The comparison between the temperature distributions for the water-based Williamson hybrid nanofluid (SWCNTs + MWCNTs)/H<sub>2</sub>O and the water-based Williamson nanofluid SWCNTs/H<sub>2</sub>O are shown in

Fig. 8. It is clearly shown the advantages of high  $\chi_{SW}$  and  $\chi_{MW}$  in the fluid enhanced temperature and its thermal boundary layer thickness.

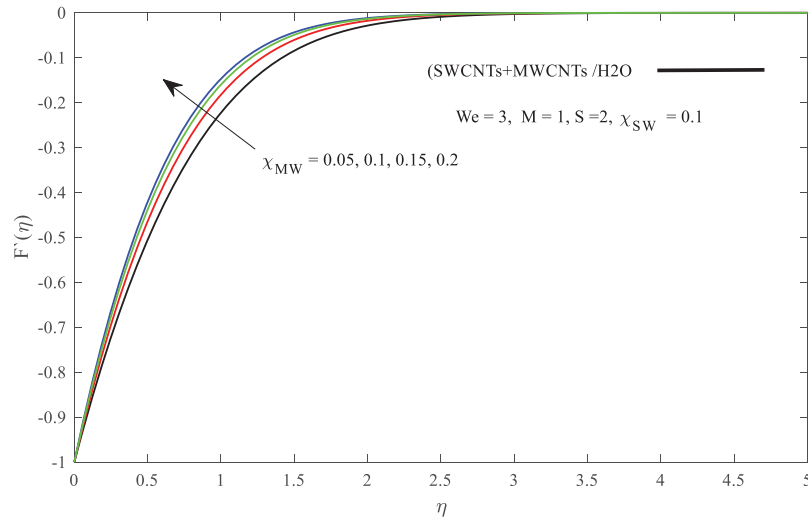


**Figure 7:** Influence of  $\chi_{MW}$  on velocity profiles  $F'(\eta)$

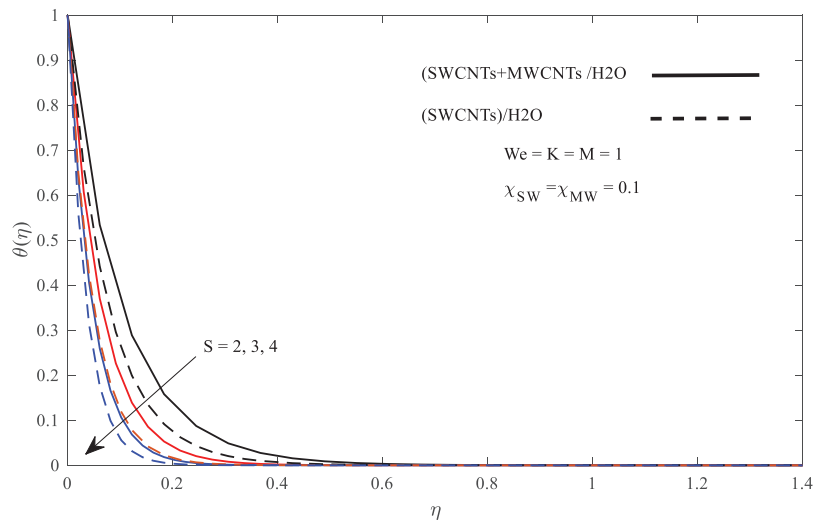


**Figure 8:** Influence of  $S$  on temperature profiles  $\theta(\eta)$

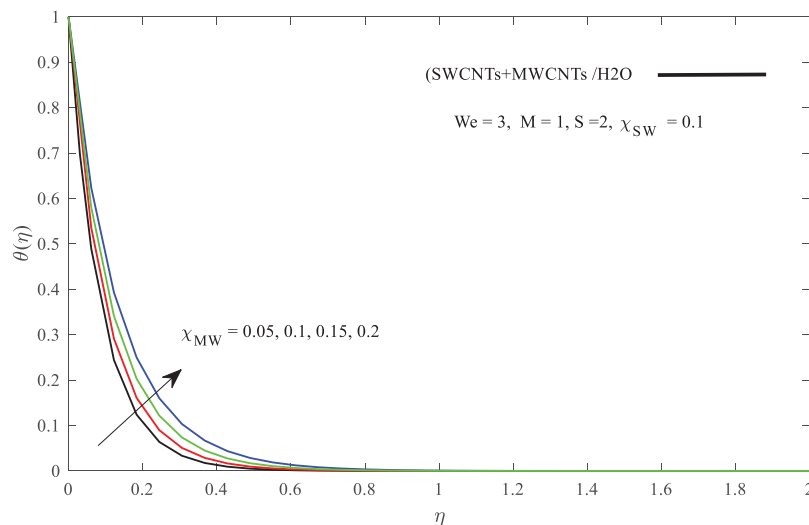


**Figure 9:** Influence of  $\chi_{MW}$  on temperature profiles  $\theta(\eta)$

## 5 Conclusions

The study on the flow and heat transfer of porous Williamson hybrid nanofluid on an exponentially shrinking sheet with magnetohydrodynamic (MHD) effects are numerically studied. The influence of the fluid parameters such as the permeability parameter  $K$ , the magnetic parameter  $M$ , the Williamson parameter  $We$ , the nanoparticle volume fractions of SWCNTs  $\chi_{SW}$  and MWCNTs nanoparticles  $\chi_{MW}$ , respectively and the wall mass transfer parameter  $S$  on the fluid flow and heat transfer characteristic are analyzed and discussed. In conclusion, it is found that:

- The increase in  $M$ ,  $K$ ,  $\chi_{MW}$ , and  $S$  has promoted the increase in skin friction coefficient while  $We$  do the contrary.
- The small increase has been recorded on a Nusselt number as  $M$  and  $K$  increase.
- $S$  played an important role as it increased may boost the values of Nusselt number drastically. Meanwhile, the Nusselt number reduced with the increase of  $We$  and  $\chi_{MW}$ .
- The water-based Williamson hybrid nanofluid (SWCNTs + MWCNTs)/H<sub>2</sub>O has a lower Nusselt number compared to the water-based Williamson nanofluid SWCNTs/H<sub>2</sub>O. This might be explained by the increase in fluid thermal conductivity in the fluid thus increasing the domination of conduction over the convection heat flow.
- The increase in magnetic parameter in SWCNTs + MWCNTs hybrid nanofluid results to the increase of 72.2% on skin friction compared to SWCNT nanofluid.

We note that this analysis may be extended for the Jeffrey fluid, Oldroyd-B fluid and other non-Newtonian fluids.

**Acknowledgement:** Authors are grateful to acknowledge the Ajloun National University for providing the facilities support.

**Funding Statement:** The authors received no specific funding for this study.

**Author Contributions:** Alkawasbeh T. H Formal Analysis, Investigation, and Methodology; Software and Validation; Muhammad K. A. M Writing—Review and editing. All authors reviewed the results and approved the final version of the manuscript.

**Availability of Data and Materials:** The data used in this paper can be requested from the corresponding author upon request.

**Conflicts of Interest:** The authors declare that they have no conflicts of interest to report regarding the present study.

## References

1. Wong, K. V., de Leon, O. (2010). Applications of nanofluids: Current and future. *Advances in Mechanical Engineering*, 2, 519659.
2. Choi, S. U., Eastman, J. A. (1995). *Enhancing thermal conductivity of fluids with nanoparticles*. IL, USA: Argonne National Lab.
3. Aladdin, N. A. L., Bachok, N., Pop, I. (2020). Cu-Al<sub>2</sub>O<sub>3</sub>/water hybrid nanofluid flow over a permeable moving surface in presence of hydromagnetic and suction effects. *Alexandria Engineering Journal*, 59(2), 657–666.
4. Zainal, N. A., Nazar, R., Naganthran, K., Pop, I. (2021). MHD flow and heat transfer of hybrid nanofluid over a permeable moving surface in the presence of thermal radiation. *International Journal of Numerical Methods for Heat & Fluid Flow*, 31(3), 858–879.
5. Prasad, P. D., Kumar, R. K., Varma, S. (2018). Heat and mass transfer analysis for the MHD flow of nanofluid with radiation absorption. *Ain Shams Engineering Journal*, 9(4), 801–813.
6. Lee, C., Choi, K., Leavitt, R., Eastman, L. (1995). Infrared hot-electron transistor with a narrow bandpass filter for high temperature operation. *Applied Physics Letters*, 66(1), 90–102.
7. Sundar, L. S., Sharma, K. V., Singh, M. K., Sousa, A. (2017). Hybrid nanofluids preparation, thermal properties, heat transfer and friction factor—A review. *Renewable and Sustainable Energy Reviews*, 68, 185–198.
8. Waini, I., Ishak, A., Pop, I. (2019). Unsteady flow and heat transfer past a stretching/shrinking sheet in a hybrid nanofluid. *International Journal of Heat and Mass Transfer*, 136, 288–297.
9. Sreedevi, P., Sudarsana, R. P., Chamkha, A. (2020). Heat and mass transfer analysis of unsteady hybrid nanofluid flow over a stretching sheet with thermal radiation. *SN Applied Sciences*, 2(7), 1222–12237.
10. Yashkun, U., Zaimi, K., Bakar, N. A. A., Ishak, A., Pop, I. (2020). MHD hybrid nanofluid flow over a permeable stretching/shrinking sheet with thermal radiation effect. *International Journal of Numerical Methods for Heat & Fluid Flow*, 31(3), 1014–1031.
11. Anuar, N., Bachok, N., Pop, I. (2018). A stability analysis of solutions in boundary layer flow and heat transfer of carbon nanotubes over a moving plate with slip effect. *Energies*, 11(12), 3243.
12. Hayat, T., Muhammad, K., Alsaedi, A., Asghar, S. (2018). Numerical study for melting heat transfer and homogeneous-heterogeneous reactions in flow involving carbon nanotubes. *Results in Physics*, 8, 415–421.
13. Zaki, A. M. M., Mohammad, N. F., Soid, S. K., Mohamed, M. K. A., Jusoh, R. (2021). Effects of heat generation/absorption on a stagnation point flow past a stretching sheet carbon nanotube water-based hybrid nanofluid with newtonian heating. *Malaysian Journal of Applied Sciences*, 6(2), 34–47.
14. Idrees, M., Shah, S. A. A., Ahmad, B., Ali, B., Mahmood, I. (2022). New insights into the heat transfer dynamics of a hybrid (SWCNT-MWCNT) nanofluid: A case of 3D rotational flow. *International Communications in Heat and Mass Transfer*, 138, 106311.
15. Crane, L. J. (1970). Flow past a stretching plate. *Zeitschrift für angewandte Mathematik und Physik ZAMP*, 21, 645–647.

16. Sulochana, C., Sandeep, N. (2016). Stagnation point flow and heat transfer behavior of Cu-water nanofluid towards horizontal and exponentially stretching/shrinking cylinders. *Applied Nanoscience*, 6, 451–459.
17. Raju, R. S., Reddy, G. J., Rao, J. A., Rashidi, M., Gorla, R. S. R. (2016). Retracted: Analytical and numerical study of unsteady MHD free convection flow over an exponentially moving vertical plate with heat absorption. *International Journal of Thermal Sciences*, 107, 303–315.
18. Jusoh, R., Nazar, R., Pop, I. (2019). Magnetohydrodynamic boundary layer flow and heat transfer of nanofluids past a bidirectional exponential permeable stretching/shrinking sheet with viscous dissipation effect. *Journal of Heat Transfer*, 141(1), 1–10.
19. Alkawasbeh, H. T., Abu-Ghurra, S., Alzgoool, H. A. (2019). Similarity solution of heat transfer for the upper-convected Maxwell casson fluid over a stretching/shrinking sheet with thermal radiation. *JP Journal of Heat and Mass Transfer*, 16, 1–17.
20. Zokri, S. M., Arifin, N. S., Mohamed, M. K. A., Salleh, M. Z., Kasim, A. R. M. et al. (2017). Influence of radiation and viscous dissipation on magnetohydrodynamic Jeffrey fluid over a stretching sheet with convective boundary conditions. *Malaysian Journal of Fundamental and Applied Sciences*, 13(3), 279–284.
21. Shah, S. A. A., Ahammad, N. A., Ali, B., Guedri, K., Awan, A. U. et al. (2022). Significance of bio-convection, MHD, thermal radiation and activation energy across Prandtl nanofluid flow: A case of stretching cylinder. *International Communications in Heat and Mass Transfer*, 137, 106299.
22. Narayana, P. V., Babu, D. H., Babu, M. S. (2019). Numerical study of a Jeffrey fluid over a porous stretching sheet with heat source/sink. *International Journal of Fluid Mechanics Research*, 46(2), 187–197.
23. Alwawi, F. A., Alkawasbeh, H. T., Rashad, A., Idris, R. (2020). MHD natural convection of sodium alginate casson nanofluid over a solid sphere. *Results in Physics*, 16, 102818.
24. Alazwari, M. A., Abu-Hamdeh, N. H., Goodarzi, M. (2021). Entropy optimization of first-grade viscoelastic nanofluid flow over a stretching sheet by using classical keller-box scheme. *Mathematics*, 9(20), 2563.
25. Kumar, R. N., Jyothi, A., Alhumade, H., Gowda, R. P., Alam, M. M. et al. (2021). Impact of magnetic dipole on thermophoretic particle deposition in the flow of Maxwell fluid over a stretching sheet. *Journal of Molecular Liquids*, 334, 116494.
26. Swalmeh, M. Z., Alkawasbeh, H. T., Hussanan, A., Nguyen, T. T., Mamat, M. (2022). Microstructure and inertial effects on natural convection micropolar nanofluid flow about a solid sphere. *International Journal of Ambient Energy*, 43(1), 666–677.
27. Zokri, S. M., Arifin, N. S., Yusof, Z. M., Sukri, N. M., Kasim, A. R. M. et al. (2022). Carboxymethyl cellulose based second grade nanofluid around a horizontal circular cylinder. *CFD Letters*, 14(11), 119–128.
28. Wan, R. W., Mohamed, M. K. A., Sarif, N., Mohammad, N. F., Soid, S. K. (2022). Blood conveying ferroparticle flow on a stagnation point over a stretching sheet: Non-Newtonian Williamson hybrid ferrofluid. *Journal of Advanced Research in Fluid Mechanics and Thermal Sciences*, 97(2), 175–185.
29. Devi, S. U., Devi, S. P. A. (2017). Heat transfer enhancement of Cu-Al<sub>2</sub>O<sub>3</sub>/water hybrid nanofluid flow over a stretching sheet. *Journal of the Nigerian Mathematical Society*, 36(2), 419–433.
30. Jusoh, R., Nazar, R., Pop, I. (2019). Magnetohydrodynamic boundary layer flow and heat transfer of nanofluids past a bidirectional exponential permeable stretching/shrinking sheet with viscous dissipation effect. *Journal of Heat Transfer*, 141(1), 012406.
31. Jamaludin, A., Naganthran, K., Nazar, R., Pop, I. (2020). Thermal radiation and MHD effects in the mixed convection flow of Fe<sub>3</sub>O<sub>4</sub>-water ferrofluid towards a nonlinearly moving surface. *Processes*, 8(1), 95.
32. Bing, K. Y., Jusoh, R., Salleh, M. Z., Hisyam, A. M., Zainuddin, N. (2023). Magnetohydrodynamics flow of Ag-TiO<sub>2</sub> hybrid nanofluid over a permeable wedge with thermal radiation and viscous dissipation. *Journal of Magnetism and Magnetic Materials*, 565, 170284.
33. Yap, B. K., Rahimah, J., Salleh, M. Z., Mohd, H. A., Nooraini, Z. (2022). Magnetohydrodynamics Ag-Fe<sub>3</sub>O<sub>4</sub>-ethylene glycol hybrid nanofluid flow and heat transfer with thermal radiation. *CFD Letters*, 14(11), 88–101.